Title

Self-Assembly of Filamentous Amelogenin Requires Calcium and Phosphate: From Dimers via Nanoribbons to Fibrils

Journal

Biomacromolecules, 13(11)

ISSN

1525-7797

Authors

Martinez-Avila, Olga
Wu, Shenping
Kim, Seung Joong
et al.

Publication Date

2012-11-12

DOI

10.1021/bm300942c

Peer reviewed

Published in final edited form as:
Biomacromolecules. 2012 November 12; 13(11): 3494–3502. doi:10.1021/bm300942c.

Self-assembly of Filamentous Amelogenin Requires Calcium and Phosphate: From Dimers via Nanoribbons to Fibrils

Olga Martinez-Avila[1], **Shenping Wu**[2], **Seung Joong Kim**[3], **Yifan Cheng**[2], **Feroz Khan**[1], **Ram Samudrala**[4], **Andrej Sali**[3], **Jeremy A. Horst**[5], and **Stefan Habelitz**[1,*]

[1]Department of Preventative and Restorative Dental Sciences, 707 Parnassus Ave., San Francisco, CA 94143, University of California

[2]Department of Biochemistry & Biophysics, 600 16th Street, Room S312B, San Francisco, CA 94158 University of California

[3]Department of Bioengineering and Therapeutic Sciences, Department of Pharmaceutical Chemistry, and California Institute for Quantitative Biosciences, Byers Hall Room 503B, 1700 4th Street, San Francisco, CA 94158 University of California

[4]Department of Microbiology, 208 Rosen Building, Box 357735 · Seattle WA 98195 University of Washington

[5]Department of Orofacial Sciences, 513 Parnassus Ave. San Francisco, CA 94143 University of California

Abstract

Enamel matrix self-assembly has long been suggested as the driving force behind aligned nanofibrous hydroxyapatite formation. We tested if amelogenin, the main enamel matrix protein, can self-assemble into ribbon-like structures in physiologic solutions. Ribbons 17nm wide were observed to grow several microns in length, requiring calcium, phosphate, and pH 4.0–6.0. The pH range suggests that the formation of ion bridges through protonated histidine residues is essential to self-assembly, supported by a statistical analysis of 212 phosphate-binding proteins predicting twelve phosphate-binding histidines. Thermophoretic analysis verified the importance of calcium and phosphate in self-assembly. X-ray scattering characterized amelogenin dimers with dimensions fitting the cross-section of the amelogenin ribbon, leading to the hypothesis that antiparallel dimers are the building blocks of the ribbons. Over 5–7 days, ribbons self-organized into bundles composed of aligned ribbons mimicking the structure of enamel crystallites in enamel rods. These observations confirm reports of filamentous organic components in developing enamel and provide a new model for matrix-templated enamel mineralization.

Keywords

Enamel; amelogenin; self-assembly; protonated histidine; biomineralization

INTRODUCTION

Self-assembly of extracellular matrix proteins results in key biological structural materials, such as collagens, keratins, and cellulose, which cells use to build entire tissues and

*Corresponding author: Stefan Habelitz, phone: 1-415-514-0818; Stefan.habelitz@ucsf.edu.

Supporting Information Available: a) SAXS data b) TEM images of control samples, including SAED of bundles of nanoribbons, c) Precision recall plot of MFS analysis. This material is available free of charge via the Internet at http://pubs.acs.org.

organs [1, 2]. The formation of dental enamel differs from this general concept as the fully developed tissue is basically free of the original organic matrix and made of 95% mineral, crystalline carbonated hydroxyapatite rendering a clear relationship between the structure of organic and inorganic components difficult. In mammalian and marsupial enamel, extremely thin (50 nm diameter) apatite fibers of several hundreds of micrometer length are packed into rods or prisms of about 5 μm width [3]. Enamel rods have species specific organization and alignment and are often separated by interrod enamel, also composed of aligned apatite nanofibers decussating enamel rods at an angle of about 60° [4]. The remarkable architectures of enamel structures suggest that a precise mechanism must have evolved that facilitated control over apatite crystallization at the nanometer length scale. The enamel matrix is generated by ameloblasts which may have an important role in organizing matrix proteins and apatite crystallites, but at the nanometer length scale it is conceivable that the matrix itself orchestrates the mineralization events and controls nucleation, growth rate, morphology and direction of growth of calcium phosphate mineral [5–8]. However, up to this date the role and the molecular mechanisms of the developing enamel matrix in synthesizing the unique architecture of mineralized enamel remain unclear.

Amelogenin proteins comprise about 90% of the organic matrix and are crucial for functional enamel development by orchestrating the mineralization of apatite crystals as shown in amelogenin deficient mice [7]. Self-assembly of amelogenin has been proposed to be critical for shaping the morphology and alignment of the growing apatite crystals [9, 10]. The human full-length amelogenin (H175) consists of 175 amino acid residues and is predominantly hydrophobic with a hydrophilic C-terminus of about 12 residues. Many structural motifs have been attributed to this protein. The molecule is intrinsically disordered in its monomeric state, but polyproline, β-turn and β-sheet like, as well α-helical elements have been reported in assembled, nanospherical structures [11–15]. Due to its hydrophobic nature, the full-length amelogenin protein has a high propensity to aggregate in aqueous solutions around its isoelectric point of 6.8 [16]. The formation of 20 to 60 nm wide nanospheres and oblates has been described in numerous studies [17]. A model which includes the formation of chain-like aggregates with the amelogenin nanosphere as building block has been developed to explain the protein's ability to generate aligned apatite nanocrystals in enamel which almost exclusively grow along their crystallographic c-axis [14, 17–20].

Previous structural studies, however, paid little attention to the effect of both calcium and phosphate ions on protein self-assembly. Amelogenin's structural development has been largely investigated in the absence of these ions or as a function of only calcium or only phosphate[9, 11, 17, 21]. In addition previous studies were performed with the assumption that amelogenin assembles within seconds or minutes. While this may be true for short peptides, proteins in general require several hours or days to form supramolecular structures [9, 11, 22, 23]. In recent studies our group took these factors into consideration as well as the amphiphilic nature of amelogenin's primary structure and developed a water-in-oil emulsion system that produced novel self-assembled structures of amelogenin. In the emulsion system amelogenin molecules stretched along the surface of micelles and were thus able to interact between the hydrophobic N-termini and facilitating the formation of nanoribbons and nanohelices [24, 25]. Nanoribbons formed at pHs between 4 and 7.5, aligned themselves, forming bundles of several micrometer width, indicating that the protein itself has the capacity to form a structure similar to the mineral crystallites in mature enamel suggesting it may be a suitable template for guiding apatite crystallization [25]. Based on these findings in an artificial system, we now further investigated the role of calcium and phosphate on self-assembly in an oil-free, aqueous environment. By careful analysis of the effect of pH on amelogenin supramolecular structure, we developed a procedure that facilitated the synthesis of amelogenin nanoribbons and under aqueous and physiological conditions. Our new model of amelogenin self-assembly is supported by a functional residue

signature analysis demonstrating the high probability of phosphate binding to histidine. Furthermore, *ab-initio* shape calculations from Small Angle X-ray Scattering (SAXS) data demonstrate the formation of amelogenin dimers which may act as building blocks for the hierarchical assembly of amelogenin nanoribbons and fibrils.

EXPERIMENTAL SECTION

Expression and purification of amelogenin

Recombinant human amelogenin rH174 and cleavage product rH146 were expressed in BL21DE3 plysS *Escherichia coli* and purified on C4 hydrophobic beads as previously described [26]. The purity of the protein batches was above 95% as assessed by HPLC. MMP-20 proteolytic product rH146 lacks 28 amino acids at the C-terminus. Recombinant amelogenin also lacks the first residue (Met) compared to the native human full-length protein H175.

Self-assembly experiments

Lyophilized proteins were dissolved in double deionized water to prepare protein stock solutions at concentration of 4–6 mg/mL. Calcium and phosphate stock solutions were prepared using reagent grade chemicals $CaCl_2$ (133.6 mM) and KH_2PO_4 (83.6 mM) and filtered (0.22 μm). Suspensions of 500μL total volume containing 0.4, 0.8, 1.2, 1.6 or 2.0 mg/mL of amelogenin rH174 were prepared by adding KH_2PO_4 in one test tube containing rH174 and $CaCl_2$ in another one with same amount of rH174. Both tubes were combined resulting in final concentrations of 0, 3.3 or 33.4 mM of $CaCl_2$ and 0, 2.1 or 20.9 mM of KH_2PO_4 and vortexed for about 30 s. The pH of resulting CaP protein solutions was initially around 2 due to residual TFA [19]. The solution was then adjusted to specific pH 3, 4.0, 4.5, 5.1, 5.5, 6.0, 6.5, 7.0, 7.4 or 8.0 (±0.1) by adding KOH. Emphasis on pH between 4 and 6 was placed because previous studies on emulsions showed higher propensity to ribbon formation at these pH [24, 25]. In addition, at pH below 6, histidine residues will protonate which may have significant influence on protein-protein and protein-mineral interactions. Protein solutions were incubated at 37 °C for up to 7 days. All samples prepared in triplicates. A volume of 2–15 μL of suspensions was extracted at different time points and prepared for a full characterization by the methods listed below [19].

Atomic force microscopy (AFM)

Extracts (15 μL) were pipetted onto microscope glass slides and kept for 1 h in a wet cell to immobilize products onto glass slide avoiding evaporation. Subsequently, samples were washed off with 1–2 drops of double deionized water, immediately dried with dust-free canned air. AFM was performed in dry conditions using tapping mode with a Nanoscope III (Digital Instruments, Santa Barbara, CA, USA) and Si-cantilevers (SSS-NCH, Nanoworld, Neuchâtel, Switzerland). The length and height of ribbons were measured from the AFM height-mode images using Nanoscope V512.r3 software and an average value determined from 50 points per sample group.

Transmission electron microscopy (TEM)

As described previously [25], a 2.0 μL drop of sample solution was adsorbed for 60 s to a glow-discharged carbon-coated copper grid (Ted Pella, Redding, CA, USA) washed off with two drops of double deionized water and air-dried. For negative staining, the TEM grid was stained with a 2% methylamine tungstate solution, pH 6.8, (NANO-W; Yaphank, NY, USA) after being washed off by two drops of water. Grids were imaged with an FEI Tenai T12 TEM (FEI company, Hillsboro, OR, USA) at 120 kV. Data were acquired with a 4 k by 4 k Gatan UltraScan CCD camera (Gatan, Pleasanton, CA, USA).

Small-angle X-Ray scattering (SAXS)

SAXS experiments were performed with the intension to detect the small units/particles in the suspension and to determine their size as a function of increasing pH in order to obtain information on possible building blocks of the nanoribbons. Protein stocks and corresponding buffers were mixed as described above at final protein concentrations of 2.0, 1.5, 1.0, 0.5, 0.25 and 0.1 mg/mL. The latter two concentrations were too diluted and did not provide sufficient scattering. In contrast, scattering was too strong when unfiltered suspensions were used, indicating the presence of high numbers of micrometer sized particles. The suspensions were therefore filtered through 0.1 μm membranes (Millipore, Bedford, MA). Protein content of the 2.0 mg/ml samples was analyzed before and after filtering using Bradford Protein Assay. Highly acidic solutions will promote monomer formation due to increased surface charges of the protein[16]. A sequential increase in pH towards neutral pH will allow us to follow the aggregation behavior of the proteins. The pH was adjusted to 1.5 (addition of HCl), 3.7, 5.6 or 7.5 (addition of KOH) in 3.3 mM of $CaCl_2$ and 2.1 mM of KH_2PO_4. SAXS measurements of rH174 and rH146 were carried out at Beam line 4-2 of the Stanford Synchrotron Radiation Lightsource. All SAXS profiles were collected at 15 °C after 24 to 48 hours of sample preparation and incubation at 37 °C. Suitable spectra were obtained at multiple concentrations from 0.5 to2 mg/mL. 5% glycerol was added to reduce radiation damage. Controls without protein but 5% glycerol were also analyzed [27].

Modeling

The *ab-initio* shapes of amelogenin (rH146 and rH174) monomers and dimers were initially calculated from a merged experimental SAXS profile by running DAMMIF 20 times and refined with additional 50 DAMMIN runs [28], followed by superposition and averaging with DAMAVER [29]. Fitting of *ab-initio* shapes into the TEM images was visualized by customized scripts in UCSF Chimera [30].

Meta-Functional Signature

A meta-functional signature (MFS[31]) compilation was built to estimate the probability for each residue in a given protein to bind soluble phosphate ions (mfsPO4), as was done previously for calcium binding [32]. Nonlocal contact predictions were combined with one dimensional predictions of conservation and structural features, by training a logistic regression to maximize scores for 591 phosphate binding among 39,641 residues in 190 proteins. Proteins were selected from all crystal diffraction structures in the Protein Databank [33][accessed May 10th, 2010] by presence of a phosphate ion noncovalently bound to the side chains of at least two residues (within a half Ångstrom of van der Waals distance). The set was filtered for non-redundancy by starting with the highest resolution (<2.1 Å) structures and progressively adding proteins to maximize diversity and maintain <30% sequence identity.

A ten-fold cross validation benchmark experiment was performed to assess the accuracy of the mfsPO4 methodology. PO4-binding residues were considered positive instances and all other residues were considered negative instances for training in a logistic regression of sequence-derived structural features, as described previously [31]. The 212 proteins were randomly distributed into ten 10% subsets. Each subset of proteins was used to test the accuracy of the mfsPO4 method when trained on the remaining 90%. Ten regressions were constructed, each with an input data set of 191 or 190 proteins (4/5 shared with the other sets), and tested on the 21 or 22 proteins not included in the input set. Since no protein was tested more than once, each test is independent and analyses can be graphed together. Depiction of performance is illustrated by a precision recall plot. The regression trained on all 212 proteins (mfsPO4) and the mfsCa method described previously [32] were applied to the

H175 amelogenin sequence. The methods were applied to 1000 proteins which are not known to bind phosphate or calcium ions. Scores of three standard deviations above the mean for these nonbinding proteins defined the threshold for binding predictions.

Microscale Thermophoresis (MST)

Thermophoresis was used to measure the binding interactions between labeled and unlabelled rH174 molecules using a Monolith NT.115 (NanoTemper Technologies GmbH, Munich, Germany) [34]. Amelogenin rH174 was labeled with a red fluorescent dye (Monolith NT™) that uses N-Hydroxysuccinimide (NHS)– ester. Free dye was removed by purification on a Sephadex G-25 column and the labeled protein was suspended in double deoinized water and freeze dried, then resuspended in acetonitrile 30% - 0.1 trifluoroacetic acid, freeze dried. Protein was then dissolved in reaction buffer at pH 2 containing 33.4 mM of $CaCl_2$ and 20.9 mM of KH_2PO_4. pH was adjusted to pH values of 2, 4.5 or 5.6. Control experiments were carried out under the same buffer conditions in the absence of CaP. For each binding assay, the concentration of the labeled rH174 is kept constant at 30 nM (1μg/ml), whereas unlabeled rH174 was titrated in a set of serial dilutions from the nanomolar to the submilimolar (100 μM ≈ 2mg/ml) range.

Results

In this study, we followed the development of self-assembled structures of amelogenin rH174 in solutions with and without calcium and phosphate ions at *p*H between 2 and 8 over a period of 7 days, using TEM and AFM analyses. Initially the characteristic spherical assemblies of amelogenin varying in size between 10 and 25 nm were observed (Figure 1A) [9]. In the absence of calcium and phosphate ions, amelogenin nanospheres were stable, though they tended to become more heterogeneous in size over time, spanning diameters of 10 to 50 nm (Figure 1B). In agreement with previous studies we observed on rare occasions that nanospheres lined up to form chains of spheres (data not shown) [18]. The structural development of amelogenin assemblies was severely altered when 3.3 or 33.4 mM calcium chloride and 2.1 or 20.9 mM potassium phosphate were added to the amelogenin suspensions in the pH-range of 4.0 to 6.0. At pH 4.5, low numbers of amelogenin nanospheres were initially observed at 24 hours of incubation, non-homogeneously distributed over the TEM grid. During this time period short ribbons developed occasionally and both ribbons and spheres were observed by TEM (Figure 1C). With continued incubation nanospheres completely disappeared while the numbers of nanoribbons increased. At day 3, nanoribbons were the only protein structure observed (Figure 1D). Most of the ribbons were still short with an average length of about 250 nm, including ribbons up to 800 nm long. At day 5, ribbons became more organized and domains of groups of ribbons in the parallel orientation became evident (Figure 1E). After 7 days, ribbons had formed larger aggregates that resembled fibrils or bundles (Figures. 1, F and G). These bundles measured between 500 nm and 2 μm in width and reached several micrometers in length consisting of continuous ribbons in parallel alignment. The bundles were surrounded by shorter segments of ribbons that appeared to be in the process of being added, thus elongating the ribbons (Figure 1H, inlet of 1G) as suggested in our previous study using an oil-water system [25]. When either phosphate (20.9 or 2.1mM) or calcium (33.4 or 3.3 mM) were added to the protein suspensions individually but not combined, no ribbons were observed within 7 days of incubation. Instead spherical and not well defined aggregates developed over time (Figure S1 B and C).

The importance of calcium ions for self-assembly was illustrated when EDTA was added to suspensions that contained amelogenin ribbons (Figure 1I). Ribbons disintegrated after EDTA exposure for 2 h, while nanospheres of about 20 nm diameters developed, indicating

that the removal of calcium destabilizes the ribbon structure and promotes nanosphere formation.

Ribbon formation was examined as a function of *p*H for samples incubated for 7 days at concentrations of 0.4 mg/mL rH174. The lowest *p*H at which ribbons self-assembled was *p*H 4.0, producing short ribbons of 200 to 500 nm length with weak alignment (Figure 2A). At day 7, ribbons and bundles of aligned ribbons were observed at *p*H 4.5, 5.1 (not shown), 5.6 and 6.0 (Figure 2, B and C). Ribbons were absent at acidic *p*H of 2.0 and 3.0 and mainly showed a diffuse protein mass without any defined structural features (Figure S1C). At *p*H 7.0, 7.4, and 8.0, a significant amount of calcium phosphate mineral formed, rendering the observation of amelogenin supramolecular structures more difficult (Figure. S1D). There is currently no evidence that amelogenin nanoribbons also form at these *p*Hs under the experimental conditions used. Figures 2D and E are AFM images of amelogenin ribbons immobilized on a glass slide before and after immersion into an aqueous solution at *p*H 2. Ribbons disintegrated into short segments of about 30 nm length within 1 min of acid exposure. In contrast, when immobilized ribbons were immersed into aqueous calcium phosphate solutions at *p*H 7.0 to 8.0, nanoribbons did not disintegrate and remained stable for the 3-day time period studied (Figure 2F). For protein concentration of 0.4 mg/mL, kinetics of ribbon formation was enhanced in the *p*H range of 4.5 to 6.0, with ribbons forming within 24 hours and bundles of ribbons appearing as early as 7 days. AFM measurements determined the thickness of ribbons to be 3.4 (±0.6) nm.

In general organization into bundles of aligned nanoribbons was accelerated with increasing amelogenin rH174 concentration. Figure 3 shows a series of TEM micrographs of amelogenin supramolecular structures obtained after 6 days of incubation in calcium phosphate solutions at 37°C. For a concentration of 0.4 mg/mL, short nanoribbons were observed at low density (Figure 3A). Ribbon length, number density and their parallel alignment were elevated when 0.8 mg/mL were used (Figure 3B). At a concentration of 1.2 mg/mL, formation of bundles of ribbons was observed (Figure 3C), while large numbers of amelogenin bundles consisting of aligned ribbons had developed when concentrations of 1.6 mg/mL were used (Figure 3D). Amelogenin concentration plays a significant role in the kinetics of ribbon formation, suggesting that at concentrations comparable to the developing enamel matrix (~300 mg/mL) self-assembly might occur at much faster time-scales [5].

Microscale thermophoresis (MST) experiments [35] were conducted with emphasis on the significance of calcium and phosphate ions for protein-protein interactions at *p*H 4.5 by titrating unlabeled rH174 into suspensions containing fluorescence-labeled rH174. We observed a strong change in fluorescence intensity following a sigmoidal profile when unlabeled rH174 was added in the presence of calcium and phosphate, characteristic of strong protein-protein interactions (Figure 4A). The half maximal effective concentration (EC50) was 176 nM and a dissociation constant of 145 ±12.2 nM was determined for amelogenin interactions, corresponding to a 5 to 10-fold increased affinity compared to calcium dependent self-assembling systems, such as binding of cartilage oligomeric matrix protein to collagen [36], EcoRV endonuclease binding to DNA [37], or calmodulin protein binding to HIV [38]. In contrast, little fluorescence activity was observed in the absence of calcium and phosphate (Figure 4A), indicating that primarily non-specific interactions occurred as characteristic for protein aggregation events [34, 35].

The pH dependence of ribbon formation suggests that self-assembly is linked to protonation of a functional moiety. The most likely amino acid residue that changes protonation state in the physiological pH range is histidine (pK_a 6.0–6.5)[39]. The dependence of self-assembly upon ions indicates a functional interaction between histidine and phosphate or calcium. An earlier analysis of a 30% non-redundant set of 336 calcium-bound protein structures showed

that histidine only represents 7 of 696 calcium-binding residues [32]. Here, we repeated this analysis for a similar set of 212 phosphate-bound protein structures, and found 132 of 950 phosphate-binding residues to be histidine, second only to arginine (Figure S3). Further, by training a meta-functional signature protocol [3132] to these proteins, we were able to predict the following phosphate-binding residues in amelogenin with high confidence: 6H, 9H, 30R, 46H, 47H, 54S, 57H, 66H, 67H, 68H, 91H, 98H, 99H, 159T, 170K, 171R, 172E, 173E, 175D. Similarly, the meta-functional signature protocol trained on calcium binding sites predicts specific amelogenin residues to carry out functional interactions with calcium: including glutamic (E) and aspartic (D) acids 18E, 39E, 157D, 161E, 168D, 172E, 173E, and 175D. Figure 4B illustrates the probability for each residue in human full-length amelogenin H175 to bind to calcium or phosphate.

To assess the size and morphology of amelogenin particles during early stages of assembly, Small Angle X-ray Scattering (SAXS) profiles (Figure S2) were obtained from filtered suspensions at *p*H between 1.5 and 7.5, with or without calcium and phosphate. The protein concentration decreased by about 10% for pH 1.5 and 2.5, by 31% for pH 5.6 and by 38% for pH 7.4. Oligomeric status was estimated from the radius of gyration (R_g), maximum dimension (D_{max}) (Table S1), radial distribution functions (Figure S2), and mass calculations [40]. For the full-length human amelogenin (rH174), monomers were observed consistently at *p*H 1.5 (R_g 46.4Å, D_{max} 158Å). When both calcium and phosphate were present, particle size, as measured by R_g increased continuously until *p*H 5.6, whereupon it matched the expected dimensions and mass of a dimer (R_g 64.1Å, D_{max} 209Å). We observed similar behavior for the C-terminal truncated human amelogenin fragment (rH146) which lacks the 28 C-terminal amino acid residues of rH174, transitioning from a monomer at *p*H 1.5 (R_g 37.2Å, D_{max} 130Å) to a dimer at *p*H 5.6 (R_g 51.6Å, D_{max} 146Å), in agreement with dimensions determined by SAXS on the 20 kd native porcine amelogenin [41]. In agreement with light scattering data by others [42], rH174 and rH146 monomers were much more abundant than dimers in the absence of calcium and phosphate regardless of the *p*H (Figures S2 E, F). Dimerization in the absence of calcium phosphate may also be reduced due to the low ionic strength of the solution which reduces the aggregation propensity of amelogenin [43].

In order to construct a low-resolution model of protein structures from SAXS data, *ab-initio* shape reconstructions were performed on data obtained at *p*H 1.5 (monomers) and at *p*H 5.6 (dimers) of rH174 in the presence of calcium and phosphate (Figure 5A). Superposition of two rH174 monomers into an rH174 dimer model revealed a reasonably good fit (ccc: 0.82) when the two monomers were allowed to overlap by three quarters of their lengths in antiparallel orientation (Figure 5B). Similarly, superposition of two rH146 monomers at *p*H 1.5 into the rH146 dimer at *p*H 5.6 resulted in a slightly better fit (ccc: 0.84). We like to point out that SAXS data alone does not define the secondary structure of amelogenin. Prevalence of β-sheets in these ribbons was observed by Raman-spectroscopy previously[25], but the presented structural model of Fig. 5 is a low-resolution model and does not include information on secondary structure of amelogenin. The nanoribbon structural model takes into consideration structural information from TEM observations and measurements on ribbons made from rH174 and from rH146 further reinforces some elements of this model, like the antiparallel orientation of amelogenin molecules and the lateral C-terminal position in the dimer. We have previously produced nanoribbon assemblies of truncated amelogenin rH146 in an emulsion system [24] and were also able to produce ribbons of rH146 without the use of an oil phase by procedures very similar to the ones described in this study for rH174. Nanoribbons of rH146 (Fig. S5), do not grow to the length of rH174 ribbons and do not show parallel alignment. Importantly for the model, the width of ribbons from rH146 was 148 (±7)Å and was significantly reduced compared to those of rH174 (167 (±10)Å). Therefore we hypothesize that the C-terminus is not part of the overlap zone and is instead

oriented towards the ribbon edges in an antiparallel arrangement of the monomers (Fig. 5C). The location of the C-terminus in the assembly is further supported by the shorter superimposed SAXS-based shape of the rH146 dimer compared to rH174 dimer at *p*H 5.6 (ccc: 0.76), demonstrating that the 28 residues missing in the rH146 construct are associated with the non-overlapping region in the dimer. A side view of the nanoribbon assembly shows the interdigitated arrangement of the dimers within the structure (Fig. 5D).

The proposed models of the rH174 dimer (Fig. 5) were superimposed onto a nanoribbon visualized by TEM and restricted to the 30Å height determined by AFM [25]. The apparent repeating units shown by TEM relatively good fit with the size and shape of the SAXS dimer model (Fig. 6). The axial symmetry of the repeating units limits the possible rotational positions of the dimer, thereby defining the interfacial surfaces on the SAXS-based dimer and monomer models. The maximum length of the rH174 dimer is ~40Å longer than the width of the rH174 ribbon measured by TEM, while the maximum diameter of the rH146 dimer matches very well the width of the rH146 ribbon in TEM (Table S1). This finding indicates a conformational shift and inward folding of C-terminal residues upon self-assembly (Fig. 6).

Discussion

Self-assembly is a process in which a disordered system forms an organized, well-defined structure or pattern as a consequence of specific, local interactions among the components themselves, without external direction and differs from disorganized aggregation, random assembly, precipitation or deposition. It requires the formation of building blocks or units with specific structural motifs which are able to form residue specific non-covalent bonds generating a systematic arrangement of these units resulting in unique structures at the nanometer to micrometer length scale. This study shows that the recombinant full-length human amelogenin protein, rH174, can self-assemble into self-aligning nanoribbons and form bundles consisting of aligned amelogenin ribbons in calcium phosphate solutions. The amelogenin structures generated in this study under aqueous conditions were identical to the ones developed in metastable water in oil emulsion [25]. While in the emulsion system the alignment of amelogenin molecules along the oil-water interface was critical to prevent a hydrophobic collapse, in this study the *p*H shift and the presence of calcium and phosphate were sufficient to stabilize the protein backbone. In the oil-water system, nanoribbons formed at pH between 4 and 7.4. In contrast, under aqueous conditions nanoribbons only formed at *p*H between 4.0 and 6.0 indicating that protonation of histidine may be required for intermolecular interactions. While this pH range is lower than what has been described for the liquid phase of secretory enamel [44, 45], it is in the range of the pH widely reported for exocytic vesicles (pH 5.0–6.0) [46]. Hence dimerization of amelogenin may already occur before exocytosis. Since TEM analysis of vesicles in ameloblasts does not indicate the presence of larger filamentous entities[47], nanoribbon assembly is more likely to occur in the extracellular space which others have shown to be composed of filamentous organic structures [48–51]. During the secretory stage of amelogenesis, the continuous exocytosis of amelogenin dimers may then contribute to elongate ribbons already present in the calcium phosphate-rich milieu of the extracellular space. A more detailed analysis of developing enamel is warranted to verify this model avoiding EDTA or demineralization by strong acids which would disintegrate amelogenin nanoribbons.

Calcium ions are well known to promote self-assembly of biomolecules through ion bridges as seen in centrin, cadherin, calmodulin, laminin [52–54]. Calcium binding to rH174 by electrostatic interactions was proposed by several studies and an average of 6.5 binding sites per molecules has been calculated [55, 56]. Calcium may act as counter ion for phosphate bridges or electrostatically associate itself to acidic residues. A detailed analysis including

the use of amelogenins with mutated histidines or other possible candidates for ion bridge formation will be required to more clearly define the mechanisms that drive ion binding and ribbon assembly.

However, the concurrent dependence upon pH and specific ions indicates that self-assembly is linked to protonation of residue side chains that mediate phosphate and/or calcium binding. Sequence and structural conservation analyses (mfsCa and mfsPO4) identified only glutamic and aspartic acid residues with a high probability of interaction with calcium, and predominantly histidines for phosphate (Figure 4B). The pKa's of these residues coincide with the shifts in self-assembly observed here. The acidic residues deprotonate around the pH 1.5to 3.7, possibly causing the disintegration of self-assembled ribbons as observed at pH below 4 (Figure 2e). Histidines will be protonated at the lower pH range. While not widely studied in biomineralization, numerous critical roles are described for histidine-phosphate interactions in kinase biology [57]. A recent study demonstrated biomineral interactions for peptides including the residues proposed here, having been identified by analogous informatic analyses of a predicted amelogenin structure and hydroxyapatite-binding sequences from phage display data evolutionary selection experiments [58]. Specifically, the histidine-rich regions were the only ones to interact with hydroxyapatite, while the acid-rich regions bound strongly to calcium. A better understanding of the roles of histidine and acidic residues in calcium and phosphate interactions may be crucial to produce a complete model of amelogenin self-assembly and control over crystal growth. Using SAXS measurements on filtered suspensions, we observed that dimers become more abundant in the presence of calcium and phosphate when the pH is raised from acidic (pH 1.5) to pH 4.5 and become the dominant subunit structure at pH 5.6 and higher. The formation of dimers in suspensions of full-length amelogenin has been described by others and may not require calcium and phosphate ions [42]. Here we hypothesize that under our experimental conditions amelogenin is surrounded by a cloud of tightly associate calcium and phosphate ions preventing the monomer from folding by hydrophobic forces as the pH is raised from 2 to between 4 and 6, when protonated histidines can still bind phosphate. As a consequence, stable dimers are observed with a consistent SAXS profile enabling determination of a molecular surface outline for amelogenin (Figure 5B).

We constructed a multi-scale molecular model of amelogenin self-assembly by integrating the data from this study (Figure 6). SAXS and TEM data indicate overlapping of the molecules by about 75% in rH174 dimers (Supplementary Table). Hence all fourteen histidine residues of rH174 will be within the overlap zone. In our model the phosphate ions are in association with histidines. Interestingly their location also coincides with the ribbon center and the dark central line that is observed along the backbone of the amelogenin nanoribbons [25]. The line may thus originate from the high electron density of calcium and phosphorous atoms (Figure 6). Dimers are composed of molecules in antiparallel configuration with the hydrophilic C-terminus oriented towards the ribbon's edges. Hence electrostatic charges build at the edges and give rise to electrostatic repulsion of amelogenin nanoribbons ultimately causing their parallel alignment as predicted in our previous analysis [25]. The tendency to self-align was not observed on ribbons made from rH146 which lack the hydrophilic ends [24]. This also suggests that the observed alignment of rH174 ribbons is not an artifact of specimen dehydration for TEM and AFM analysis. The alignment of ribbons ultimately leads to the formation of bundles composed of aligned ribbons (Fig. 1D–G). Such bundles could, with the involvement of the ameloblasts, evolve into an organic precursor of the enamel rod ready for templating the formation of oriented apatite crystallization.

We observed that amelogenin nanospheres become unstable in the presence of both calcium and phosphate ions. Others have also shown that monomers and oligomers co-exists with

nanospheres and nanospheres readily release oligomers when in contact with solid surfaces [59–61]. A recent publication reported on the hierarchical assembly of amelogenin nanospheres in the absence of calcium and phosphate ions, illustrating that such nanospheres completely disappeared when calcium and phosphate were added and mineralization was initiated [11]. Other studies were also not able to show evidence of nanosphere formation once apatite mineralization occurred, further supporting our finding that amelogenin nanospheres are unstable in solutions containing mineralizing ions [18, 23].

While it has been shown previously that divalent anions like HPO_3^{2-} can act as bridges between peptide and protein molecules [62], the mechanism of assembly by ion interaction with protonated histidine as shown in this study is novel. We have observed apatite crystallization in the presence of amelogenin nanoribbons. However, the formation of such crystals was not in association with the protein template, suggesting that the ribbons themselves may not act as apatite nucleator but perhaps as a reservoir of these ions. Moreover, we observed the presence of amorphous calcium phosphate in or around bundles of ribbons (Figure S4). This finding is in agreement with the process of biomineralization, since as a common principle the secreted matrix does not induce mineralization directly without post-secretory modification (e.g. phosphorylation, proteolysis) [63, 64]. Interaction with other, non-amelogenin proteins or processing of amelogenin which are crucial to enamel formation may also be required for apatite crystallization and will be subject to future studies [65].

CONCLUSIONS

The formation of highly organized apatite crystals in dental enamel suggests that the organic matrix acts as a guide and template for mineral formation during tissue development. Here we developed a system that facilitated the formation of amelogenin nanoribbons in aqueous suspensions and describe the required physical-chemical parameters. In the presence of calcium and phosphate amelogenin nanospheres become unstable and disintegrate while gradually ribbons of specific width develop over a period of days, self-align and self-organize into micrometer sized bundles of ribbons. Ribbons of similar size and shape with a high degree of parallel alignment have been characterized by TEM analysis of the developing matrix of dental enamel [48]. Ribbon-like structures are part of many descriptions of the matrix of developing enamel [49–51]. The ability of amelogenin to form ribbons which develop into micrometer-sized bundles of aligned ribbons substantially impacts the current paradigm of amelogenin-guided mineralization of apatite in enamel and will provide critical insights into our understanding of amelogenesis as well as enhance our ability to generate enamel *in vitro* through biomimetic approaches.

Supplementary Material

Refer to Web version on PubMed Central for supplementary material.

Acknowledgments

Dr. Stefan Duhr (NanoTemper Technologies) for facilitating the use of the MST system; Tsutomu Matsui, Lester Carter and Hiro Tsuruta at Stanford Synchrotron Radiation Lightsource for their support. NIH/NIDCR for financial support through RO1-DE017529, DE017529S2 and F30-DE017522 (J. A. Horst).

References

1. Smith KH, Tejeda-Montes E, Poch M, Mata A. Chem Soc Rev. 2011; 40:4563–4577. [PubMed: 21629920]
2. Ingber DE. Sci Am. 1998; 278:48–57. [PubMed: 11536845]

3. Warshawsky H. Anat Rec. 1989; 224:242–262. [PubMed: 2672889]
4. White SN, Luo W, Paine ML, Fong H, Sarikaya M, Snead ML. J Dent Res. 2001; 80:321–326. [PubMed: 11269723]
5. Smith CE. Crit Rev Oral Biol Med. 1998; 9:128–161. [PubMed: 9603233]
6. Fincham AG, Moradian-Oldak J, Simmer JP. J Struct Biol. 1999; 126:270–299. [PubMed: 10441532]
7. Gibson CW, Yuan ZA, Hall B, Longenecker G, Chen E, Thyagarajan T, Sreenath T, Wright JT, Decker S, Piddington R, Harrison G, Kulkarni AB. J Biol Chem. 2001; 276:31871–31875. [PubMed: 11406633]
8. Paine ML, White SN, Luo W, Fong H, Sarikaya M, Snead ML. Matrix Biol. 2001; 20:273–292. [PubMed: 11566262]
9. Moradian-Oldak J. Matrix Biol. 2001; 20:293–305. [PubMed: 11566263]
10. Margolis HC, Beniash E, Fowler CE. J Dent Res. 2006; 85:775–793. [PubMed: 16931858]
11. Fang PA, Conway JF, Margolis HC, Simmer JP, Beniash E. Proc Natl Acad Sci U S A. 2011; 108:14097–14102. [PubMed: 21825148]
12. Delak K, Harcup C, Lakshminarayanan R, Sun Z, Fan Y, Moradian-Oldak J, Evans JS. Biochemistry. 2009; 48:2272–2281. [PubMed: 19236004]
13. Lakshminarayanan R, Fan D, Du C, Moradian-Oldak J. Biophys J. 2007; 93:3664–3674. [PubMed: 17704165]
14. Du C, Falini G, Fermani S, Abbott C, Moradian-Oldak J. Science. 2005; 307:1450–454. Erratum in: Science. 2005 Sep 30;309(5744):2166. [PubMed: 15746422]
15. Zhang X, Ramirez BE, Liao X, Diekwisch TG. PLoS One. 2011; 6:e24952. [PubMed: 21984897]
16. Uskokovic V, Castiglione Z, Cubas P, Zhu L, Li W, Habelitz S. J Dent Res. 2010; 89:149–153. [PubMed: 20040742]
17. Aichmayer B, Wiedemann-Bidlack FB, Gilow C, Simmer JP, Yamakoshi Y, Emmerling F, Margolis HC, Fratzl P. Biomacromolecules. 2010; 11:369–376. [PubMed: 20038137]
18. Beniash E, Simmer JP, Margolis HC. J Struct Biol. 2005; 149:182–190. [PubMed: 15681234]
19. He X, Li W, Habelitz S. J Struct Biol. 2008; 164:314–321. [PubMed: 18845261]
20. Habelitz S, Kullar A, Marshall SJ, DenBesten PK, Balooch M, Marshall GW, Li W. J Dent Res. 2004; 83:698–702. [PubMed: 15329375]
21. Lakshminarayanan R, Yoon I, Hegde BG, Fan D, Du C, Moradian-Oldak J. Proteins. 2009; 76:560–569. [PubMed: 19274734]
22. Aichmayer B, Margolis HC, Sigel R, Yamakoshi Y, Simmer JP, Fratzl P. J Struct Biol. 2005; 151:239–249. [PubMed: 16125972]
23. Wiedemann-Bidlack FB, Beniash E, Yamakoshi Y, Simmer JP, Margolis HC. J Struct Biol. 2007; 160:57–69. [PubMed: 17719243]
24. Martinez-Avila OM, Wu S, Cheng Y, Lee R, Khan F, Habelitz S. Eur J Oral Sci. 2011; 119(Suppl 1):75–82. [PubMed: 22243231]
25. He XD, Wu SP, Martinez-Avila O, Cheng YF, Habelitz S. J Struct Biol. 2011; 174:203–212. [PubMed: 21134461]
26. Li W, Gao C, Yan Y, DenBesten P. Arch Oral Biol. 2003; 48:177–183. [PubMed: 12648554]
27. Bernado P, Modig K, Grela P, Svergun DI, Tchorzewski M, Pons M, Akke M. Biophys J. 2010; 98:2374–2382. [PubMed: 20483347]
28. Svergun DI. Biophys J. 1999; 76:2879–2886. [PubMed: 10354416]
29. Volkov VV, Svergun DI. J Appl Cryst. 2003; 36:860–864.
30. Pettersen EF, Goddard TD, Huang CC, Couch GS, Greenblatt DM, Meng EC, Ferrin TE. J Comput Chem. 2004; 25:1605–1612. [PubMed: 15264254]
31. Wang K, Horst JA, Cheng G, Nickle DC, Samudrala R. PLoS Comput Biol. 2008; 4:e1000181. [PubMed: 18818722]
32. Horst JA, Samudrala R. Pattern Recogn Lett. 2010; 31:2103–2112.
33. Berman H, Henrick K, Nakamura H, Markley JL. Nucleic Acids Res. 2007; 35:D301–303. [PubMed: 17142228]

34. Jerabek-Willemsen M, Wienken CJ, Braun D, Baaske P, Duhr S. Assay Drug Dev Technol. 2011; 9:342–353. [PubMed: 21812660]
35. Wienken CJ, Baaske P, Rothbauer U, Braun D, Duhr S. Nat Commun. 2010; 1:100. [PubMed: 20981028]
36. Rosenberg K, Olsson H, Morgelin M, Heinegard D. J Biol Chem. 1998; 273:20397–20403. [PubMed: 9685393]
37. Hiller DA, Perona JJ. Biochemistry. 2006; 45:11453–11463. [PubMed: 16981705]
38. Ghanam RH, Fernandez TF, Fledderman EL, Saad JS. J Biol Chem. 285:41911–41920. [PubMed: 20956522]
39. Stryer, L. Biochemistry. 4. W.H. Freeman & Company; 1995.
40. Glatter, O.; Kratky, O. Small Angle X-ray Scattering. Academic Press; 1982.
41. Matsushima N, Izumi Y, Aoba T. J Biochem. 1998; 123:150–156. [PubMed: 9504422]
42. Buchko GW, Tarasevich BJ, Bekhazi J, Snead ML, Shaw WJ. Biochem. 2008; 47:13215–13222. [PubMed: 19086270]
43. Bromley KM, Kiss AS, Lokappa SB, Lakshminarayanan R, Fan D, Ndao M, Evans JS, Moradian-Oldak J. J Biol Chem. 2011; 286:34643–34653. [PubMed: 21840988]
44. Aoba T, Moreno EC. Calcif Tissue Int. 1987; 41:86–94. [PubMed: 3115550]
45. Lacruz RS, Nanci A, Kurtz I, Wright JT, Paine ML. Calcif Tissue Int. 2010; 86:91–103. [PubMed: 20016979]
46. Paroutis P, Touret N, Grinstein S. Physiology (Bethesda). 2004; 19:207–215. [PubMed: 15304635]
47. Nanci A, Zalzal S, Lavoie P, Kunikata M, Chen W, Krebsbach PH, Yamada Y, Hammarstrom L, Simmer JP, Fincham AG, Snead ML, Smith CE. J Histochem Cytochem. 1998; 46:911–934. [PubMed: 9671442]
48. Travis DF, Glimcher MJ. J Cell Biol. 1964; 23:447–497. [PubMed: 14245432]
49. Diekwisch TG. Connect Tissue Res. 1998; 38:101–111. [PubMed: 11063019]
50. Nanci A, Bendayan M, Slavkin HC. J Histochem Cytochem. 1985; 33:1153–1160. [PubMed: 4056379]
51. Meyer JM, Bodier-Houlle P, Cuisinier FJ, Lesot H, Ruch JV. In Vitro Cell Dev Biol Anim. 1999; 35:159–168. [PubMed: 10476913]
52. Yurchenco PD, Cheng YS. J Biol Chem. 1993; 268:17286–17299. [PubMed: 8349613]
53. Alattia JR, Ames JB, Porumb T, Tong KI, Heng YM, Ottensmeyer P, Kay CM, Ikura M. FEBS Lett. 1997; 417:405–408. [PubMed: 9409761]
54. Williams RJ. Cell Calcium. 1992; 13:355–362. [PubMed: 1505001]
55. Le TQ, Gochin M, Featherstone JD, Li W, DenBesten PK. Eur J Oral Sci. 2006; 114(Suppl 1): 320–326. [PubMed: 16674706]
56. Uskokovic V, Li W, Habelitz S. J Cryst Growth. 2011; 316:106–117.
57. Besant PG, Attwood PV. Biochim Biophys Acta. 2005; 1754:281–290. [PubMed: 16188507]
58. Gungormus M, Oren EE, Horst JA, Fong H, Hnilova M, Somerman MJ, Snead ML, Samudrala R, Tamerler C, Sarikaya M. Int J Oral Sci. 2012; 4:69–77. [PubMed: 22743342]
59. Tarasevich BJ, Lea S, Bernt W, Engelhard M, Shaw WJ. J Phys Chem B. 2009; 113:1833–1842. [PubMed: 19199690]
60. Tarasevich BJ, Lea S, Bernt W, Engelhard MH, Shaw WJ. Biopolymers. 2009; 91:103–107. [PubMed: 19025992]
61. Chen CL, Bromley KM, Moradian-Oldak J, DeYoreo JJ. J Am Chem Soc. 2011; 133:17406–17413. [PubMed: 21916473]
62. Zou D, Tie Z, Lu C, Qin M, Lu X, Wang M, Wang W, Chen P. Biopolymers. 2010; 93:318–329. [PubMed: 19885921]
63. George A, Veis A. Chem Rev. 2008; 108:4670–4693. [PubMed: 18831570]
64. Qin C, Baba O, Butler WT. Crit Rev Oral Biol Med. 2004; 15:126–136. [PubMed: 15187031]
65. Smith CE, Wazen R, Hu Y, Zalzal SF, Nanci A, Simmer JP, Hu JC. Eur J Oral Sci. 2009; 117:485–497. [PubMed: 19758243]

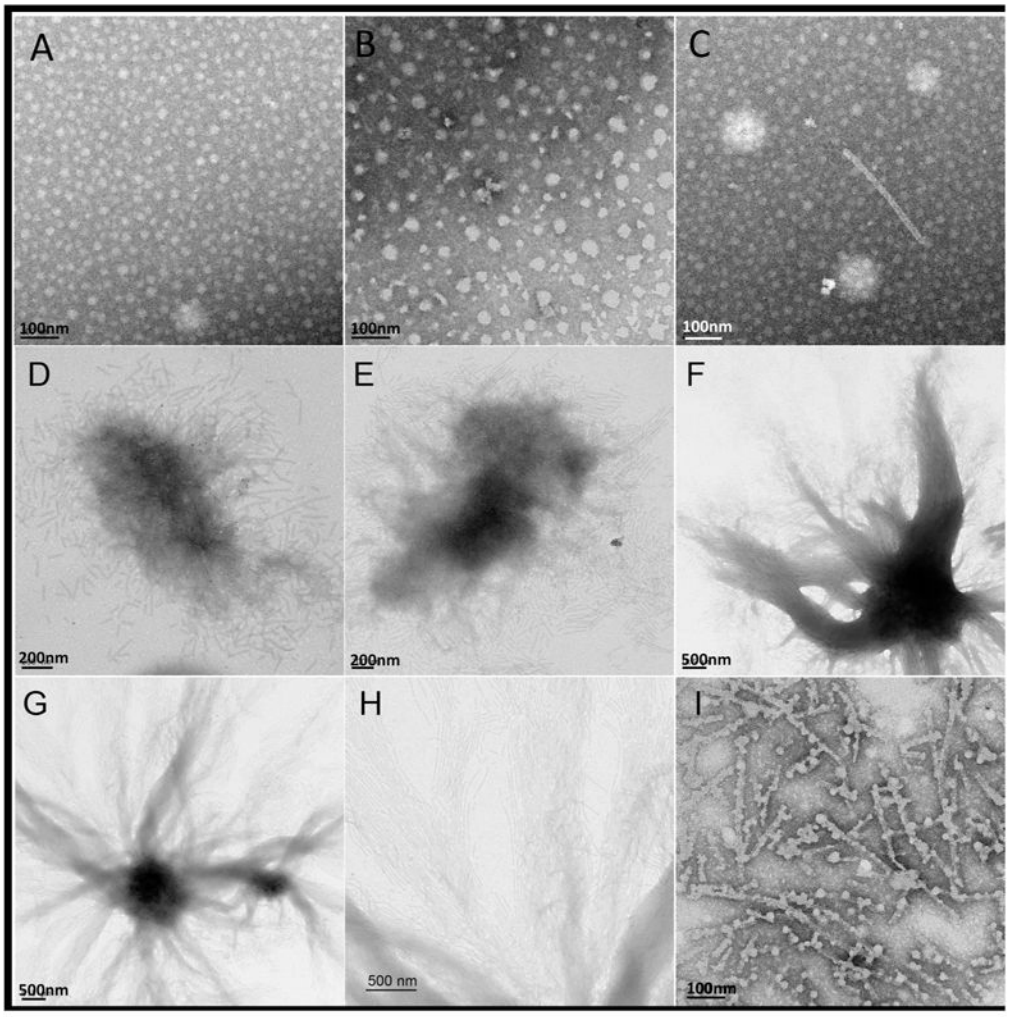

Figure 1.
TEM analysis of self-assembled structures of rH174 (0.4 mg/mL) observed at *p*H 4.5. (A) in the absence of calcium and phosphate ions at day 1 and (B) day 7 (C–H) compared to structures which develop over the same time period in the presence of calcium and phosphate: (C) day 1, shows both nanospheres and nanoribbons; (D) day 4, short ribbons of about 200–800 nm length are the only structural feature observed; (E) day 5, domains of aligned ribbons appear; (F and G) day 7, bundle-like structures containing numerous aligned ribbons appear; (H) high-resolution of (G) showing that shorter ribbon segments are present at the end of the ribbons and in process to be added to existing longer and aligned ribbons; I) ribbons exposed to 0.5 M EDTA for 2h at pH 6, showing disintegration of ribbons, resulting in the appearance of nanospheres.

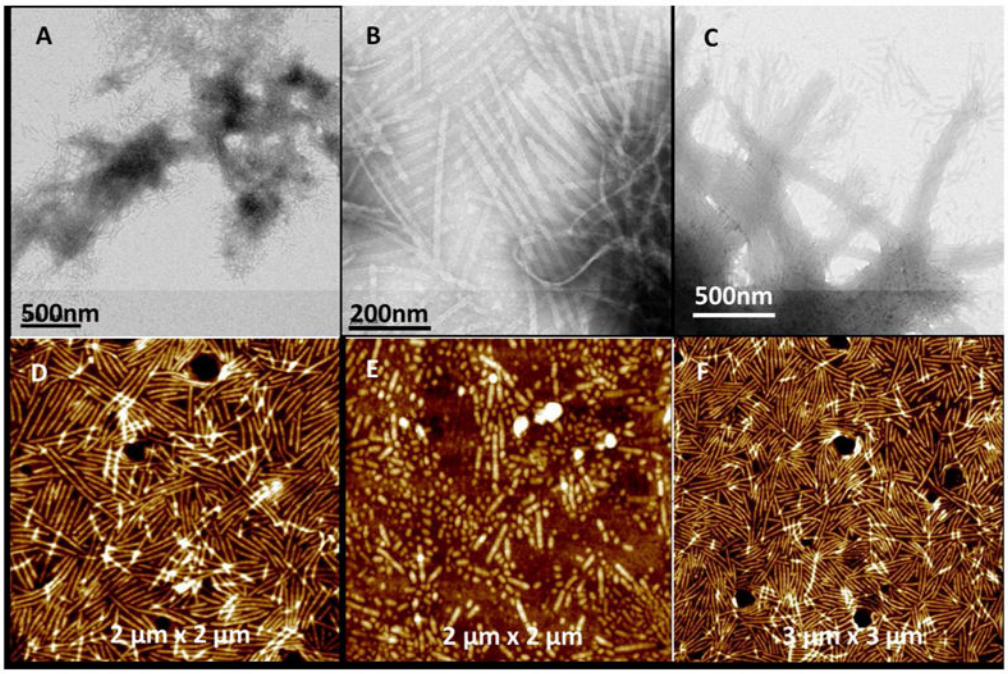

Figure 2.
TEM and AFM images of supramolecular structures of rH174 at day 7 self-assembled at different pH. (A) pH 4.0, showing short randomly oriented ribbons; (B) pH 5.5 and C) pH 6.0 ribbons have aligned and formed bundles. AFM images of (D) amelogenin nanoribbons formed at pH 4.5 and immobilized onto glass slide; E) same ribbons after rinsing with HCl-solution at pH 2, causing the ribbons to disintegrate; F) ribbons remained unchanged when exposed to buffered solutions at pH 7.0 for three days.

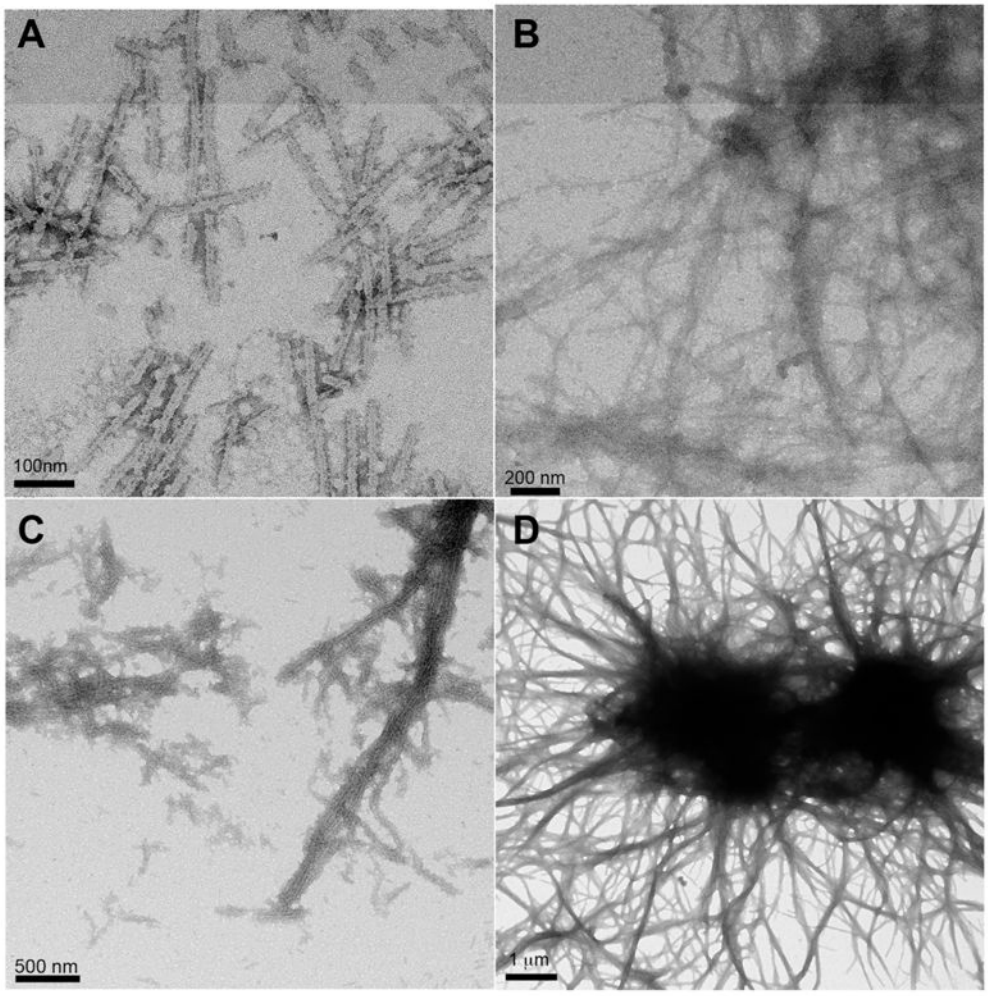

Figure 3.
TEM images of supramolecular structures of rH174 present at day 6, as a function of protein concentration at pH 4.5: (A) at 0.4 mg/mL; (B) at 0.8 mg/mL; (C) at 1.2 mg/mL and (D) at 1.6 mg/mL. Size and alignment including the formation of bundles are enhanced with increasing protein concentration.

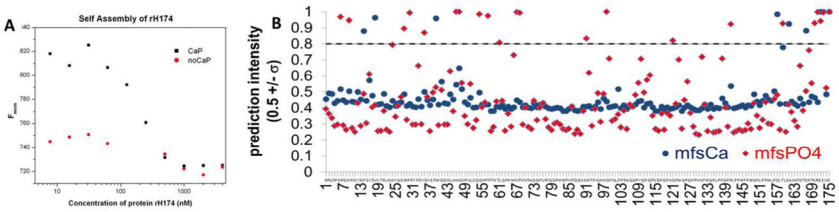

Figure 4.

Structural binding analysis of amelogenin (H175) to calcium and phosphate ions. (A) Microscale Thermophoresis (MST) experiments show a strong change in fluorescence intensity in the presence of calcium and phosphate ions when unlabeled rH174 is titrated into labeled rH174 sols at pH 4.5 (black curve); indicating strong protein-protein interaction. The change in fluorescence was not quantifiable in the absence of calcium and phosphate (red data points). (B) Meta-functional signatures (MFS) showing the probability for each residue in amelogenin H175 to bind soluble phosphate ions (mfsPO4) or soluble calcium ions (mfsCa). Scores above threshold (horizontal line) indicate high binding probablity. Threshold was set at least three standard deviations higher than the mean for all scores of non-calcium or non-phosphate binding.

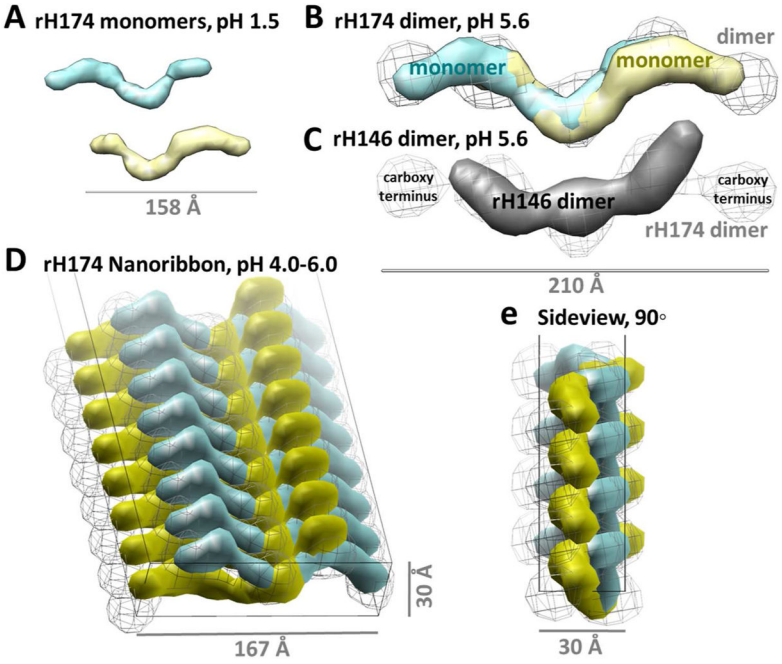

Figure 5.

Multiscale modeling of amelogenin ribbon assembly. *Ab-initio* shapes of (A) the rH174 monomer (cyan and yellow; Rg 46.4Å, Dmax 158Å) and (B) rH174 dimer (gray wire; Rg 64.1Å, Dmax 209Å) were derived from SAXS profiles measured in the presence of calcium and phosphate at pH 1.5 and pH 5.6, respectively. (B) Superimposition of SAXS-derived rH174 monomers within a rH174 dimer supports antiparallel symmetry (cross correlation coefficient = 0.82). (C) Antiparallel monomer orientation is also supported by comparison of an rH146 dimer (solid gray) superposed to an H174 dimer (CCC = 0.76), which also reveals the carboxy termini lying on the distant ends of the H174 dimer. (D), (E) Building out these dimers as units of a multimer into a flat columnar template derived from TEM and AFM measurements of the ribbons presents a mechanistic molecular model of amelogenin self-assembly.

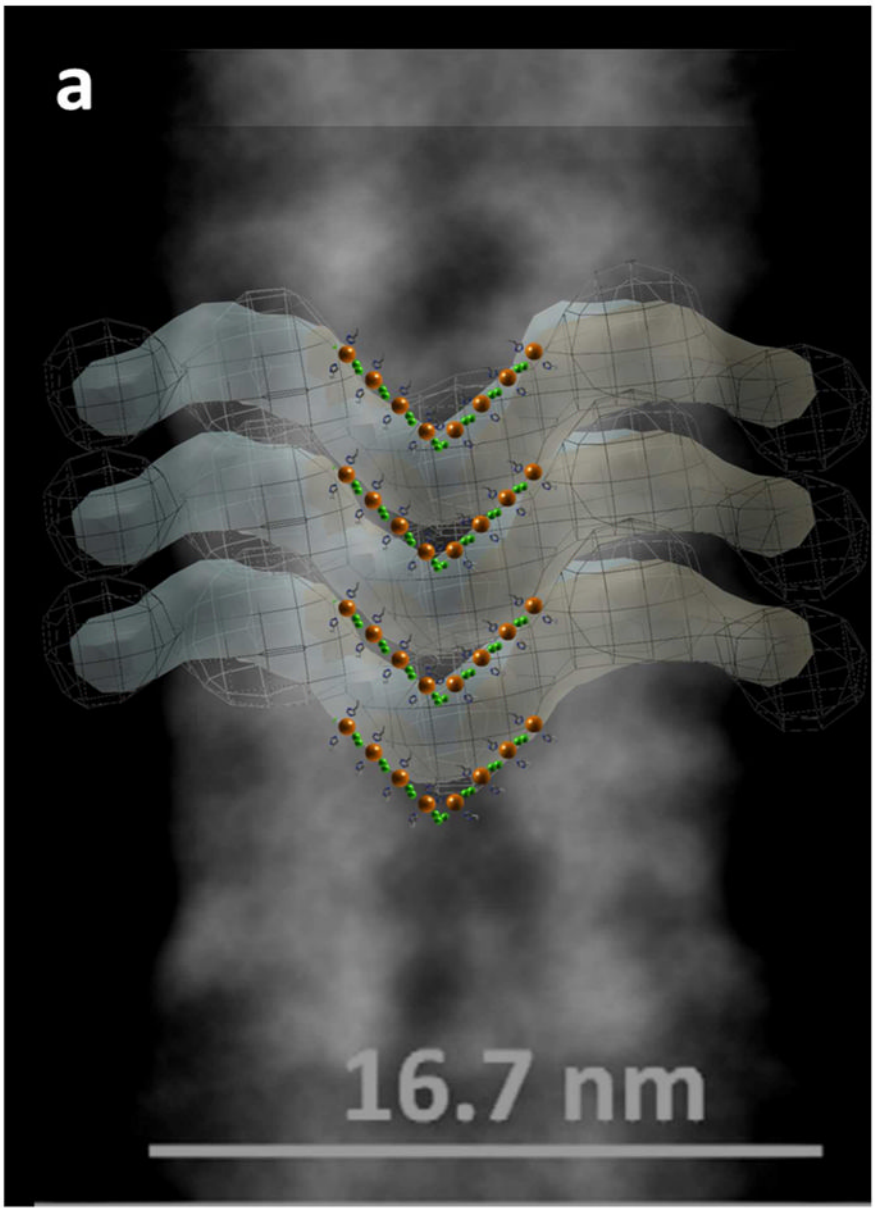

Figure 6.

Comparison of the dimer-based model to a consensus TEM overlay for amelogenin nanoribbons. The apparent repeating units observed by TEM overlay are supported by the size and shape of the SAXS dimer model. The electron dense negative stain shown in the TEM, obtained in a previous study[25], suggests buildup of calcium and phosphate along the center of the ribbon. Thus phosphates (orange) and histidines thought to carry out the pH dependent phosphate interactions are shown at the intersection of this region, with calcium ions (green) interspersed to represent potential counter ions for phosphate bridging. The coarse localization for histidines provides probabilistic tethers for future modeling efforts. The stacked orientation of amelogenin, calcium, and phosphate facilitates an explanation for the linear scaling of multimerization observed in this study. The SAXS based models of dimeric building blocks exceed the width of the ribbon as observed in the TEM by about 2nm on both sides, suggesting that the non-overlapping portion at the C-terminus may be folded inwards.